A systematic construction of gapped non-liquid states

Xiao-Gang Wen¹

Department of Physics, Massachusetts Institute of Technology, Cambridge, Massachusetts 02139, USA

Gapped non-liquid state (also known as fracton state) is a very special gapped quantum state of matter that is characterized by a microscopic cellular structure. Such microscopic cellular structure has a macroscopic effect at arbitrary long distances and cannot be removed by renormalization group flow, which makes gapped non-liquid state beyond the description of topological quantum field theory with a finite number of fields. Using Abelian and non-Abelian topological orders in 2-dimensional (2d) space and the different ways to glue them together via their gapped boundaries, we propose a systematic way to construct 3d gapped states (and in other dimensions). The resulting states are called cellular topological states, which include gapped non-liquid states, as well as gapped liquid states in some special cases. Some new fracton states with fractal excitations are constructed even using 2d \mathbb{Z}_2 topological order. More general cellular topological states can be constructed by connecting 2d domain walls between different 3d topological orders. The constructed cellular topological states can be viewed as fixed-point states for a reverse renormalization of gapped non-liquid states.

CONTENTS

1.	Introduction	1
II.	A simple construction A. The construction B. Entanglement structure	2 2 2
III.	Cellular topological states from 2+1D \mathbb{Z}_2 topological order A. A general construction B. Cellular topological state $(GT_{\mathbb{Z}_2}^{2+1},C_1,C_1)$ C. Cellular topological state $(GT_{\mathbb{Z}_2}^{2+1},C_2,C_2)$ D. Cellular topological state $(GT_{\mathbb{Z}_2}^{2+1},C_1,C_3)$ E. A cellular topological state on square column lattice F. A cellular topological state on cubic lattice	5 5 6 7 7 8 8
IV.	Reverse renormalization and generic construction	9
	References	10

I. INTRODUCTION

Different phases of matter are not only characterized by their symmetry breaking patterns. 1,2 Even systems without any symmetry can have many distinct gapped zero-temperature phases, characterized by different patterns of long range quantum entanglement³. Those gapped phases include $gapped\ liquid\ phases^{4,5}$ [which incluse phases with topological orders $^{6-8}$, symmetry enriched topological (SET) orders $^{9-17}$ and symmetry protected trivial (SPT) orders $^{18-20}$], as well as $gapped\ non-liquid\ phases^{21,22}$, such as foliated phases 4,23,24 (i.e. type-I fracton phases 25).

So far, we have a nearly complete understanding gapped liquid phases for boson and fermion systems with and without symmetry. In 1+1D, all gapped phases are liquid phases. They are classified by $(G_H, G_{\Psi}, \omega_2)^{26,27}$, where G_H is the symmetry group of the Hamiltonian, G_{Ψ}

the symmetry group of the ground state $G_{\Psi} \subset G_H$, and $\omega_2 \in H^2(G_{\Psi}, \mathbb{R}/\mathbb{Z})$ is a group 2-cocycle for the unbroken symmetry group G_{Ψ} .

In 2+1D, we believe that all gapped phases are liquid phases. They are classified (up to E_8 invertible topological orders and for a finite unitary on-site symmetry G_{Ψ}) by $(G_H, \mathcal{R}ep(G_{\Psi}) \subset \mathcal{C} \subset \mathcal{M})$ for bosonic systems and by $(G_H, s\mathcal{R}ep(G_{\Psi}) \subset \mathcal{C} \subset \mathcal{M})$ for fermionic systems $^{28-30}$. Here $\mathcal{R}ep(G_{\Psi})$ is symmetric fusion category formed by representations of G_{Ψ} , and $s\mathcal{R}ep(G_{\Psi})$ is symmetric fusion category formed by \mathbb{Z}_2^f -graded (i.e. fermion graded) representations of G_{Ψ} . Also \mathcal{C} is a braided fusion category and \mathcal{M} is a minimal modular extension 29,30 .

In 3+1D, some gapped phases are *liquid phases* while others are non-liquid phases. The 3+1D gapped liquid phases without symmetry for bosonic systems (i.e. 3+1D bosonic topological orders) are classified by Dijkgraak-Witten theories if the point-like excitations are all bosons, by twisted 2-gauge theory with gauge 2-group $\mathcal{B}(G,\mathbb{Z}_2)$ if some point-like excitations are fermions and there are no Majorana zero modes, and by a special class of fusion 2-categories if some point-like excitations are fermions and there are Majorana zero modes at some triple-string intersections^{31–33}. Comparing with classifications of 3+1D SPT orders for bosonic^{20,34} and fermioinc systems^{35–40}, this result suggests that all 3+1D gapped liquid phases (such as SET and SPT phases) for bosonic and fermionic systems with a finite unitary symmetry (including trivial symmetry, *i.e.* no symmetry) are classified by partially gauging the symmetry of the bosonic/fermionic SPT orders³².

However, the classification of gapped non-liquid phases is still unclear (for a review, see Ref. 41). In this paper, we are going to propose a very systematic construction of 3+1D gapped non-liquid phases for bosonic and fermionic systems with possible symmetry. We hope our systematic construction can lead to a classifying understanding of gapped non-liquid phases. Our construction is based on the above classification of gapped liquid phases and a classification of gapped boundaries of those gapped liquid

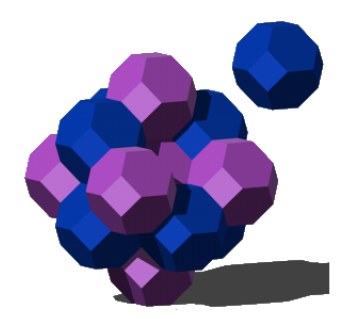


FIG. 1. The 3d space is divided into cells. Each cell surface is occupied by a 2+1D topological order. Each edge is occupied by an anomalous 1+1D topological order, which is a gapped boundary of a stacking of the 2+1D topological orders.

phases 42 .

In a simplified form of our construction, we divide the 3d space into cells (see Fig. 1), where only cell surfaces can overlap. We put a 2+1D topological order on each patch of overlapping surfaces. The edges can be viewed as a boundary of several stacked 2+1D topological orders. We put a gapped boundary (a 1+1D anomalous topological order $^{42-44}$) on each edge. We refer to the constructed gapped states as **cellular topological states**, to stress the intrinsic cellular structure (such as foliation structure 4,23,24) in those gapped states. In general, cellular topological states are gapped non-liquid states, although some special cellular topological states can be liquid states (*i.e.* the cellular structure disappears).

Our construction is similar to some constructions of SPT and SET phases^{45–48}. It is also similar to the layer, cage-net, or string-membrane constructions of fracton phases^{49–54}. However, there are some important differences, which allow us to construct new fracton states with fractal excitations,²² even starting from 2+1D \mathbb{Z}_2 topological order.

We like to mention that there are also gapless non-liquid phases. They include Fermi liquid in 2+1D and above, 5 as well as some models with emergent graviton-like excitations. $^{55-57}$

II. A SIMPLE CONSTRUCTION

A. The construction

We first consider a very simple decomposition of the 3d space into hexagonal column's $\mathbb{R}^3 = \bigcup_i (H_i \times \mathbb{R}_z)$, where H_i are non-overlaping hexagons whose union form the x-y plane. (see Fig. 2). We use i,j to label the vertices and ij the links of honeycomb lattice in the x-y plane. We then, put bosonic topological orders M_{ij} without symmetry on the faces of hexagonal column's $\langle ij \rangle \times \mathbb{R}_z$.

We note that the vertical line at the vertex i of the honeycomb lattice is the boundary of the topological order $\mathsf{M}_{ij} \boxtimes \mathsf{M}_{ik} \boxtimes \mathsf{M}_{il}$. (Here $\mathsf{C} \boxtimes \mathsf{D}$ is the topological order

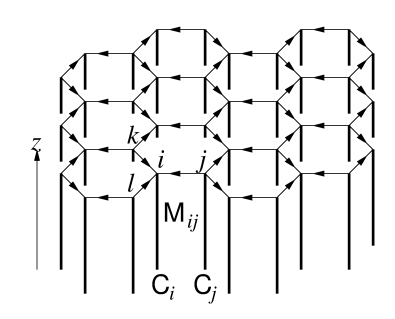


FIG. 2. The 3d space is decomposed into hexagonal column's. The honeycomb lattice has two kinds of vertices: type-A vertices have arrows pointing in, and type-B vertices have arrows pointing out.

obtained by stacking topological orders C and D.) So in general, we can put a 1+1D anomalous topological order $^{42-44}$ on the vertical line i which is described by a fusion category $\mathsf{C}_i{}^{58}.$ Those fusion categories satisfy

$$\mathsf{Bulk}(\mathsf{C}_i) = \begin{cases} \mathsf{M}_i, & \text{if } i \text{ is type-A,} \\ \overline{\mathsf{M}}_i, & \text{if } i \text{ is type-B,} \end{cases}$$
$$\mathsf{M}_i = \mathsf{M}_{ij} \boxtimes \mathsf{M}_{ik} \boxtimes \mathsf{M}_{il}, \tag{1}$$

which means that 1+1D anomalous topological order C_i is a gapped boundary of 2+1D topological order M_i or $\overline{M_i}^{42,59-61}$. Here Bulk is the holographic map that map a boundary anomalous topological order to its unique corresponding bulk topological order. ^{42,62-64} Bulk is closely related to the Drinfeld center, whose physical calculation is presented in Ref. 58. Also, the bar means the time reversal conjugate.

We see that, using the data $(\mathsf{M}_{ij},\mathsf{C}_i)$, we can construct a 3+1D gapped phases for bosonic systems, which can be a non-liquid gapped phase. In general M_{ij} can be non-Abelian topological orders.

We like to mention that if, for example, C_i has a form

$$C_i = D_i \boxtimes E_i,$$

$$Bulk(E_i) = M_{ii}, \quad Bulk(D_i) = M_{ik} \boxtimes M_{il}, \quad (2)$$

then the layer M_{ij} is not connected to the line at vertex-i. Such a layer can shrink to the line at vertex-j on the other side (see Fig. 3), and hence can be removed (or correspond to trivial M_{ij} case). Thus we are looking for the so called entangled solutions of eqn. (1) that do not have the form (2). We also like to mention that the gapped boundaries of a 2+1D topological order can be constructed via anyon condensation and are classified by the Lagrangian algebra of the 2+1D topological order $^{65-70}$.

B. Entanglement structure

To understand the cellular topological state in Fig. 2 better, we like to study the entanglement structure of the

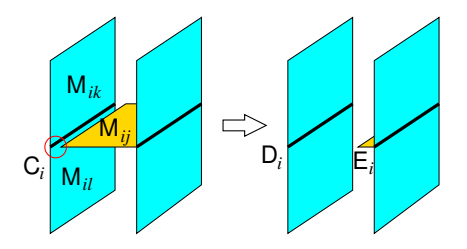


FIG. 3. For C_i satisfying eqn. (2), the layer M_{ij} is detached.

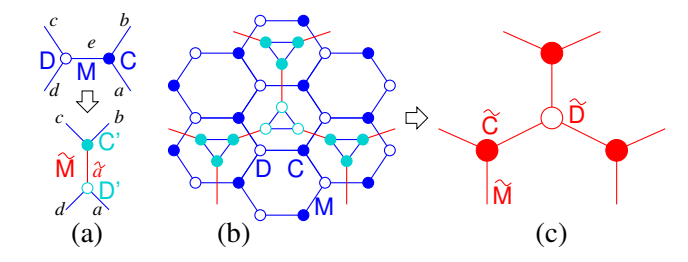


FIG. 4. (a) A deformation step $C \boxtimes_M D = C' \boxtimes_{\tilde{M}} D'$ (see eqn. (11)). (b) Using the deformation step, we can change the blue-hexagonal tensor network to the one formed by red links and light-blue dots. (c) Shrinking the triangles to the red dots produces the blue-hexagonal tensor network (see eqn. (12)). This completes a renormalization step $(M, C, D) \to (\tilde{M}, \tilde{C}, \tilde{D})$.

cellular topological state. The entanglement structure can be revealed by the renormalization of the state (see Fig. 4). The renormalization is done via a basic deformation step in Fig. 4a, where fusing two boundaries C, D and fusing two boundaries C', D' given rise to the same boundary of the four stacked 2+1D topological orders (described by the four outer lines): $C \boxtimes_M D = C' \boxtimes_{\tilde{M}} D'$.

To describe such a deformation step more explicitly, we need a quantitative description of the 2+1D topological order M_{ij} and the 1+1D anomalous topological order C_i . The topological orders can be characterized by the representations of mapping class groups for all Riemannian surfaces.^{7,8} Here for simplicity,^{71–73} we will only use the representation for mapping class group of a torus. 74,75 In other words, we will use the S_a^b, T_a^b matrices (the generators of a modular representation of $SL(2,\mathbb{Z})$ to characterize a 2+1D topological order M, where a, b label the types of the topological excitations in the topological order. Similarly, the gapped domain walls C between two topological orders characterized by (S,T) and (S',T') are characterized by the wave function overlap of the degenerate ground states, $|\psi_a\rangle$ and $|\psi'_{a'}\rangle$, of the two topological orders on torus: 61

$$\langle \psi'_{a'} | e^{-H_W} | \psi_a \rangle = e^{-\sigma A_{T^2} + o(\frac{1}{A_{T^2}})} C_{a'}^a$$
 (3)

where H_W is local hermitian operator like a Hamiltonian of a quantum system, A_{T^2} is the area of the torus T^2 and $C_{a'}^a$ is a topological invariant that characterize the domain between the two topological orders. $C_{a'}^a$ turns out

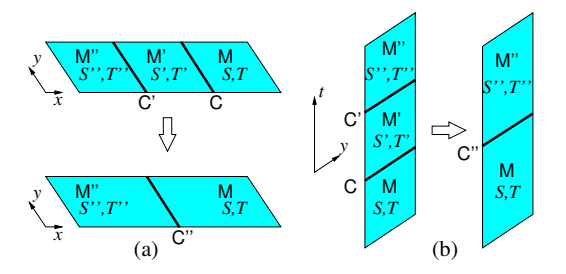


FIG. 5. (a) Fusion of two 1+1D domain walls C and C' connected by a 2+1D topological order M' gives rise to $C'' = C' \boxtimes_{M'} C$. The loop-like t-direction is not shown. (b) Exchanging x and t, we get the corresponding wave function overlapes. Two wave function overlaps C and C' can be reduced to one wave function overlap C''. The loop-like x-direction is not shown.

to be non-negative integers for torus, which satisfy^{59,61}

$$\sum_{b'} S'^{b'}_{a'} C^b_{b'} = \sum_{a} C^a_{a'} S^b_{a}, \qquad \sum_{b'} T'^{b'}_{a'} C^b_{b'} = \sum_{a} C^a_{a'} T^b_{a},$$

$$C^a_{a'} C^b_{b'} \le \sum_{c',c} N^{a'b'}_{c'} C^c_{c'} N^{ab}_{c}.$$
(4)

where N_c^{ab} and $N_{c'}^{a'b'}$ are the fusion coefficients for the topological excitations in the two topological orders.

Now let us describe an elementary deformation step. Consider three topological orders M, M' and M" characterized by (S,T), (S',T'), and (S'',T''). A tensor C describes a domain wall C between (S,T) and (S',T'), and a tensor C' describes a domain wall C' between (S',T') and (S'',T''). The two domain wall C and C' can fuse into a single domain wall C" (see Fig. 5a):

$$\mathsf{C}'' = \mathsf{C}' \boxtimes_{\mathsf{M}'} \mathsf{C}. \tag{5}$$

Note the C and C' are fused with a "glue" M' (see Fig. 5)^{62,63}, which is indicated by the subscript of \boxtimes . It turns out that the domain wall C" is characterized by a tensor C''

$$(C'')_{a''}^a = \sum_{a'} (C')_{a''}^{a'} C_{a'}^a, \text{ or } C'' = C'C.$$
 (6)

The above just describes the composition of wavefunction overlap in Fig. 5b.

We note that the above elementary step is reversible, which can fuse two domain walls or split a single domain wall. A fusion followed a split in a different direction produces the elementary deformation step in Fig. 4a.

If one side of the domain wall between M and M' is trivial (say M' is trivial), then the domain wall (i.e. the boundary of M) is described by $C_1^a \equiv C^a$ (or by $C_a^1 \equiv C_a$ if the boundary is at the opposite side of M, where 1 corresponds to the trivial excitation). We see that the boundary C_i in our construction (see Fig. 2) is charac-

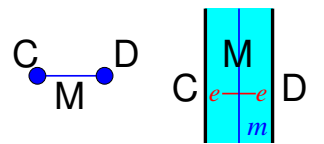


FIG. 6. A simple tensor network formed by two vertices connected by a link. The link corresponds to a 2+1D topological order M. The vertices corresponds to a 1+1D anomalous topological order $\mathsf{C},\mathsf{D}.$

terized by non-negative integer tensor

$$\mathsf{C}_{i} \sim \begin{cases} C_{a_{ij}a_{ik}a_{il}}, & \text{if } i \text{ is type-A}, \\ C^{a_{ij}a_{ik}a_{il}}, & \text{if } i \text{ is type-B}, \end{cases} \tag{7}$$

where (a_{ij}, a_{ik}, a_{il}) labels the topological excitations in $\mathsf{M}_i = \mathsf{M}_{ij} \boxtimes \mathsf{M}_{ik} \boxtimes \mathsf{M}_{il}$ and a_{ij} labels the topological excitations in M_{ij} etc.

The above discussion suggests that we can view the blue honeycomb lattice in Fig. 4 as a tensor network, where the tensors at the solid-blue vertices are given by $C^{a_{ij}a_{ik}a_{il}}$, while the tensors at the open-blue vertices are given by $D_{a_{ij}a_{ik}a_{il}}$. The link $\langle ij \rangle$ carries the index a_{ij} which label the types of topological excitations in M_{ij} . The trace of the tensor network give us the partition function, which is the ground state degeneracy of the cellular topological state. ^{59,61,67}

To see why trace of tensor network give rise to ground state degeneracy, let us consider a simple tensor network with two vertices connected by a link 59,67 . The link corresponds to a \mathbb{Z}_2 topological order $\mathsf{M} = \mathsf{GT}_{\mathbb{Z}_2}^{2+1}$ (i.e. the $2+1\mathsf{D}$ \mathbb{Z}_2 gauge theory) 76,77 . The \mathbb{Z}_2 topological order $\mathsf{GT}_{\mathbb{Z}_2}^{2+1}$ has four type of topological excitations $\mathbf{1}, e, m, f$, labeled by a=1,2,3,4 respectively. The S,T modular matrices are given by

The \mathbb{Z}_2 topological order has two gapped boundayies: C_e from e-particle condensation and C_m from m-particle condensation⁶⁶. There are described by the following rank-1 tensors $(a=1,\cdots,4)$

$$C_e: (C_e^a) = \begin{pmatrix} 1\\1\\0\\0 \end{pmatrix}, \quad C_m: (C_m^a) = \begin{pmatrix} 1\\0\\1\\0 \end{pmatrix}$$
 (9)

If both boundaries in Fig. 6 are given by $C = D = C_e$, then the ground state degeneracy of the system is given by $\sum_a C_e^a C_e^a = 2$. This result can also be obtained using the e-string operator W_e that creates a pairs of e-particle

at its ends, and the m-string operator W_m that creates a pairs of m-particle at its ends. Since e-particles condense at the boundaries, the open e-string operator, W_e , connecting the two boundaries does change the energy (i.e. commute with the Hamiltonian). A loop of the m-string operator in z-direction, W_m^z , also commute with the Hamiltonian. Since the e-string operator and the m-string operator intersect at one point and anti-commute $W_eW_m^z = -W_m^zW_e$, the ground states are 2-fold degenerate.

If the boundaries in Fig. 6 are given by $C = C_e$ and $C = C_m$, then the ground state degeneracy of the system is given by $\sum_a C_e^a C_m^a = 1$. In this case, there is no string operators that connect the two boundaries and create two condensing particles.

With the above tensor representation of the boundaries, the renormalization of the cellular topological state becomes the standard renormalization of tensor network. ^{78,79} Let us assume that, in the hexagonal tensor network (see Fig. 2 and 4b), all M_{ij} are the same $M_{ij} = M$, whose topological excitations are labeled by a, b, c, \cdots . The boundaries C_i at the solid-bule vertices are given by $C_i = C$ (or by tensor C^{abc}), while boundaries C_i at the open-bule vertices are given by $C_i = D$ (or by tensor D_{abc}). For simplicity, we will assume

$$C^{abc} = C^{cab}, \quad D_{abc} = D_{cab}. \tag{10}$$

Then, the deformation in Fig. 4a is explicitly given by the following tensor relation:

$$\sum_{e} C^{eab} D_{ecd} = \sum_{\tilde{a}} (C')^{\tilde{a}bc} (D')_{\tilde{a}da}. \tag{11}$$

where \tilde{a} label the topological excitations in a new 2+1D topological order $\tilde{\mathsf{M}}$. We like to mention that the deformation (11) is not unique. There can be many choices of $\tilde{\mathsf{M}},\mathsf{C}',\mathsf{D}'$ that satisfy eqn. (11). We like to find the deformation where $\tilde{\mathsf{M}}$ has minimal total quantum dimension $D = \sqrt{\sum_{\tilde{a}} d_{\tilde{a}}^2}$. Here $d_{\tilde{a}}$ is the quantum dimensions of topological excitations in $\tilde{\mathsf{M}}$. Later, we will see that if the resulting $\tilde{\mathsf{M}}$ is trivial or equal to the original M , then the corresponding cellular topological state may be a liquid state.

We like to remark that, as we will see later, a cellular state contains extra local structures that are not related to the universal class of a gapped state. So, by choosing M to have minimal total quantum dimension, we hope to obtain the simplest cellular topological state after each step of renormalization, trying to remove those local structures as much as possible.

We can use the deformation Fig. 4a to deform the blue hexagonal tensor network in Fig. 4b to the one described by red links in Fig. 4b. We then shrink the small triangles in Fig. 4b to a point and obtain a new red hexagonal tensor network in Fig. 4c. The new boundaries \tilde{C} and \tilde{D}

are given by

$$\tilde{C}^{\tilde{a}\tilde{b}\tilde{c}} = \sum_{a,b,c} (C')^{\tilde{a}cb} (C')^{\tilde{b}ac} (C')^{\tilde{c}ba},
\tilde{D}_{\tilde{a}\tilde{b}\tilde{c}} = \sum_{a,b,c} (D')_{\tilde{a}cb} (D')_{\tilde{b}ac} (D')_{\tilde{c}ba}.$$
(12)

The two relations (11) and (12) define the renormalization of the cellular topological state.

III. CELLULAR TOPOLOGICAL STATES FROM 2+1D \mathbb{Z}_2 TOPOLOGICAL ORDER

A. A general construction

In this section, we are going to construct some simple cellular topological states in Fig. 2 by choosing M_{ij} to be the same 2+1D \mathbb{Z}_2 topological order $M_{ij} = \mathsf{GT}_{\mathbb{Z}_2}^{2+1}$. We find that $\mathsf{GT}_{\mathbb{Z}_2}^{2+1} \boxtimes \mathsf{GT}_{\mathbb{Z}_2}^{2+1} \boxtimes \mathsf{GT}_{\mathbb{Z}_2}^{2+1}$ has 10 types of gapped boundaries, $\mathsf{Bulk}(\mathsf{C}_i) = \mathsf{GT}_{\mathbb{Z}_2}^{2+1} \boxtimes \mathsf{GT}_{\mathbb{Z}_2}^{2+1} \boxtimes \mathsf{GT}_{\mathbb{Z}_2}^{2+1}$, that are entangled (*i.e.* do not have the form in eqn. (2)). Their tensor representations, C_i^{abc} , are givein by (only non-zero elements are listed):

$$\begin{split} \mathsf{C}_1: C_1^{111}, C_1^{122}, C_1^{212}, C_1^{221}, C_1^{333}, C_1^{344}, C_1^{434}, C_1^{443} &= 1, \\ \mathsf{C}_2: C_2^{111}, C_2^{144}, C_2^{223}, C_2^{232}, C_2^{232}, C_2^{333}, C_2^{414}, C_2^{441} &= 1, \\ \mathsf{C}_3: C_3^{111}, C_3^{133}, C_3^{222}, C_3^{244}, C_3^{313}, C_3^{331}, C_3^{424}, C_3^{442} &= 1, \\ \mathsf{C}_4: C_4^{111}, C_4^{144}, C_4^{222}, C_4^{233}, C_4^{232}, C_4^{323}, C_4^{344}, C_4^{441} &= 1, \\ \mathsf{C}_5: C_5^{111}, C_5^{132}, C_5^{212}, C_5^{231}, C_5^{232}, C_5^{344}, C_4^{424}, C_4^{423} &= 1, \\ \mathsf{C}_6: C_6^{111}, C_6^{132}, C_6^{223}, C_6^{244}, C_6^{312}, C_6^{331}, C_6^{424}, C_6^{443} &= 1, \\ \mathsf{C}_7: C_7^{111}, C_7^{123}, C_7^{213}, C_7^{221}, C_7^{322}, C_7^{344}, C_4^{474}, C_7^{442} &= 1, \\ \mathsf{C}_8: C_8^{111}, C_8^{123}, C_8^{232}, C_8^{244}, C_8^{313}, C_8^{321}, C_8^{434}, C_8^{442} &= 1, \\ \mathsf{C}_9: C_9^{111}, C_9^{133}, C_9^{213}, C_9^{231}, C_9^{322}, C_9^{344}, C_9^{424}, C_9^{442} &= 1, \\ \mathsf{C}_{10}: C_{10}^{111}, C_{10}^{122}, C_{10}^{233}, C_{10}^{244}, C_{10}^{312}, C_{10}^{321}, C_{10}^{434}, C_{10}^{443} &= 1. \\ \end{split}$$

The first four, (C_1, C_2, C_3, C_4) , are cyclic symmetric (10). Let us examine those four types of the boundaries of $\mathsf{GT}_{\mathbb{Z}_2}^{2+1} \boxtimes \mathsf{GT}_{\mathbb{Z}_2}^{2+1} \boxtimes \mathsf{GT}_{\mathbb{Z}_2}^{2+1}$ in more details. First we note that C_1 and C_3 as well as C_2 and C_4 differ by an automorphism of the \mathbb{Z}_2 topological order: $e_i \leftrightarrow m_i$, where i=1,2,3 labels the three \mathbb{Z}_2 topological orders in $\mathsf{GT}_{\mathbb{Z}_2}^{2+1} \boxtimes \mathsf{GT}_{\mathbb{Z}_2}^{2+1} \boxtimes \mathsf{GT}_{\mathbb{Z}_2}^{2+1}$. Those boundaries are formed by condensing the topological excitations in the three \mathbb{Z}_2 topological orders $^{66,68-70}$. In the following, we list the condensing excitations (the generators) for the four boundaries:



FIG. 7. If we choose $\tilde{M}=M\boxtimes M,$ then eqn. (11) always has solutions.

which are obtained from the tensor indices abc with $C^{abc} = 1$.

If we assume \tilde{M} to be the trival topological order, then the equation eqn. (11) for the deformation in Fig. 11a has no solutions, for those cyclic symmetric boundaries. If we assume \tilde{M} to be given by the 2+1D \mathbb{Z}_2 topological order $\mathsf{GT}_{\mathbb{Z}_2}^{2+1}$, then for the following (C,D) 's

$$(C_1, C_2), (C_1, C_3), (C_1, C_4), (C_2, C_3), (C_3, C_4), (15)$$

the deformation eqn. (11) also has no solution. But, for other cyclic symmetric boundaries C,D 's, the deformation eqn. (11) has two solutions, which are given by (see Fig. 11)

$$\begin{split} (C,D) &= (C_1,C_1) \to (C',D') = (C_1,C_1) \text{ or } (C_{10},C_{10}), \\ (C,D) &= (C_3,C_3) \to (C',D') = (C_3,C_3) \text{ or } (C_9,C_9), \\ (C,D) &= (C_2,C_2) \to (C',D') = (C_2,C_2) \text{ or } (C_4,C_4), \\ (C,D) &= (C_4,C_4) \to (C',D') = (C_2,C_2) \text{ or } (C_4,C_4), \\ (C,D) &= (C_2,C_4) \to (C',D') = (C_2,C_4) \text{ or } (C_4,C_2). \end{split}$$

If we choose \tilde{M} to be a more general topological order, such as $\tilde{M} = M \boxtimes M$, then eqn. (11) always has solutions (see Fig. 7).

After obtaining C' and D', we can perform the shrinking operation (12) (see Fig. 4) to obtain \tilde{C}, \tilde{D} :

$$\begin{split} (\mathsf{C},\mathsf{D}) &= (\mathsf{C}_1,\mathsf{C}_1) \to (\tilde{\mathsf{C}},\tilde{\mathsf{D}}) = (2\mathsf{C}_1,2\mathsf{C}_1) \text{ or } (2\mathsf{C}_3,2\mathsf{C}_3), \\ (\mathsf{C},\mathsf{D}) &= (\mathsf{C}_3,\mathsf{C}_3) \to (\tilde{\mathsf{C}},\tilde{\mathsf{D}}) = (2\mathsf{C}_3,2\mathsf{C}_3) \text{ or } (2\mathsf{C}_1,2\mathsf{C}_1), \\ (\mathsf{C},\mathsf{D}) &= (\mathsf{C}_2,\mathsf{C}_2) \to (\tilde{\mathsf{C}},\tilde{\mathsf{D}}) = (2\mathsf{C}_2,2\mathsf{C}_2) \text{ or } (2\mathsf{C}_4,2\mathsf{C}_4), \\ (\mathsf{C},\mathsf{D}) &= (\mathsf{C}_4,\mathsf{C}_4) \to (\tilde{\mathsf{C}},\tilde{\mathsf{D}}) = (2\mathsf{C}_2,2\mathsf{C}_2) \text{ or } (2\mathsf{C}_4,2\mathsf{C}_4), \\ (\mathsf{C},\mathsf{D}) &= (\mathsf{C}_2,\mathsf{C}_4) \to (\tilde{\mathsf{C}},\tilde{\mathsf{D}}) = (2\mathsf{C}_2,2\mathsf{C}_4) \text{ or } (2\mathsf{C}_4,2\mathsf{C}_2). \end{split}$$

Here $2C \equiv C \oplus C$ means that the boundary is formed by accidentally degenerate C and C. Since \tilde{C} comes from fusing three C's. We roughly have a fusion rule for the boundaries: $C \boxtimes C \boxtimes C \sim \tilde{C}$. The results (17) suggest that the boundary C and D have a quantum dimension $\sqrt{2}$. So the ground state degeneracy is roughly given by $2^{\frac{N_A+N_B}{2}}$ (up to a finite factor), where N_A and N_B are the number of type-A and type-B vertices (see Fig. 2). In other words the ground state degeneracy is roughly given by 2^{N_h} where N_h is the number of the hexagons (see Fig. 2).

In our above discussions, we have assumed that the vertices in the honeycomb lattice (see Fig. 2) is far apart. This leads to the accidentally degeneracy of two C's. However, in reality, the vertices in the honeycomb lattice have a small separation. In this case, the degeneracy of two C's is split.

To summarize, we constructed five cellular topological phases labeled by the following (M,C,D)'s:

$$(\mathsf{GT}^{2+1}_{\mathbb{Z}_2},\mathsf{C}_1,\mathsf{C}_1), \ (\mathsf{GT}^{2+1}_{\mathbb{Z}_2},\mathsf{C}_2,\mathsf{C}_2), \ (\mathsf{GT}^{2+1}_{\mathbb{Z}_2},\mathsf{C}_3,\mathsf{C}_3), \\ (\mathsf{GT}^{2+1}_{\mathbb{Z}_2},\mathsf{C}_4,\mathsf{C}_4), \ (\mathsf{GT}^{2+1}_{\mathbb{Z}_2},\mathsf{C}_2,\mathsf{C}_4).$$
 (18)

Those phases have the key properties that under the renormalization $(M,C,D)\to (\tilde{M},\tilde{C},\tilde{D})$ in Fig. 4, we cannot reduce the 2+1D topological order M to the trivial one, but M can be unchanged under renormalization: $M=GT_{\mathbb{Z}_2}^{2+1}\to \tilde{M}=GT_{\mathbb{Z}_2}^{2+1}.$ Later, we will see that the invariance of M under renormalization suggests that the corresponding cellular topological state is a liquid state.

We also constructed five cellular topological phases labeled by the following (M,C,D)'s:

$$(\mathsf{GT}^{2+1}_{\mathbb{Z}_2},\mathsf{C}_1,\mathsf{C}_2), \ (\mathsf{GT}^{2+1}_{\mathbb{Z}_2},\mathsf{C}_1,\mathsf{C}_3), \ (\mathsf{GT}^{2+1}_{\mathbb{Z}_2},\mathsf{C}_1,\mathsf{C}_4), \\ (\mathsf{GT}^{2+1}_{\mathbb{Z}_2},\mathsf{C}_2,\mathsf{C}_3), \ (\mathsf{GT}^{2+1}_{\mathbb{Z}_2},\mathsf{C}_3,\mathsf{C}_4).$$
 (19)

Those phases have the key properties that under the renormalization $(M,C,D) \to (\tilde{M},\tilde{C},\tilde{D})$ in Fig. 4, we cannot reduce the 2+1D topological order M to the trivial one, and M cannot be unchanged under the renormalization. Later, we will see that the non-invariance of M under renormalization suggests that the corresponding cellular topological state is a non-liquid state.

B. Cellular topological state $(GT_{\mathbb{Z}_2}^{2+1}, C_1, C_1)$

Some cellular topological states are non-liquid states, while other cellular topological states are actually liquid states. In this section, we are going to discuss a cellular topological state $(\mathsf{GT}_{\mathbb{Z}_2}^{2+1},\mathsf{C}_1,\mathsf{C}_1)$, and show that it is actually a gapped liquid state – a 3+1D \mathbb{Z}_2 topological ordered state $\mathsf{GT}_{\mathbb{Z}_2}^{3+1}$ described by \mathbb{Z}_2 gauge theory.

The cellular topological state $(\mathsf{GT}_{\mathbb{Z}_2}^{2+1},\mathsf{C}_1,\mathsf{C}_1)$ is constructed using 2+1D \mathbb{Z}_2 topological order, and choosing the junction of three \mathbb{Z}_2 topological orders to be the 1+1D anomalous topological order C_1 in eqn. (13) (see Fig. 2).

The 1+1D topological order C_1 has a condensation of e_1e_2 , e_2e_3 , and e_3e_1 , for the excisions in the connected 2+1D topological order. This means that the e-particles can freely move between the 2+1D topological orders $\mathsf{GT}^{2+1}_{\mathbb{Z}_2}$ connected by the 1+1D topological order C_1 (see Fig. 8). In other words, the e-particle can move freely in the whole 3d space.

From the renormalization of the corresponding tensor network

$$(C, D) = (C_1, C_1) \to (\tilde{C}, \tilde{D}) = (2C_1, 2C_1),$$
 (20)

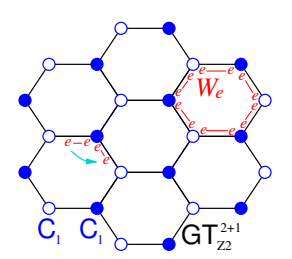


FIG. 8. In the cellular topological state $(\mathsf{GT}^{2+1}_{\mathbb{Z}_2},\mathsf{C}_1,\mathsf{C}_1)$, the e-particle can move freely in 3d space. The unmarked links are in sector-1. A configuration with a loop of links in sector-2 (marked by e-e) corresponds to another degenerate ground state.

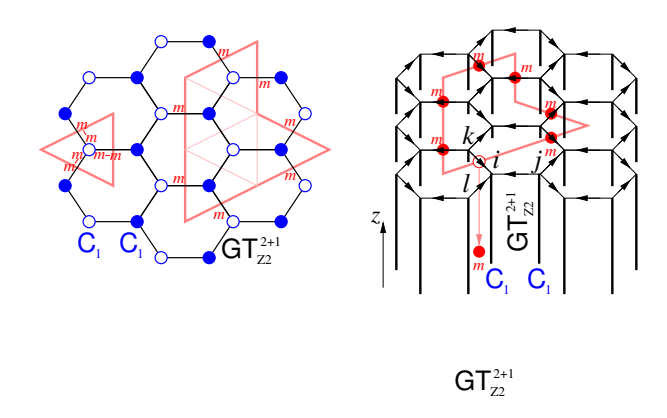


FIG. 9. In the cellular topological state $(\mathsf{GT}^{2+1}_{\mathbb{Z}_2},\mathsf{C}_1,\mathsf{C}_1)$, the m-particles must form a closed loop in the dual honeycomb lattice.

we find that the ground state degeneracy is roughly given by 2^{N_h} . Such degeneracy can be understood by using the closed e-string operator W_e that move an e-particle around a hexagon and the closed m-string operators W_m^z that wraps around in the z-direction (see Fig. 6). Both closed string operators commute with the Hamiltonian. Since W_e and W_m^z anti-commute when they intersects, we find that each hexagon contributes a factor 2 (corresponding to $W_e = \pm 1$) to the ground state degeneracy.

The cellular topological state has a tensor network representation (see Fig. 2 and 4). We can also compute ground state state degeneracy using the trace of the tensor network. Each link of the tensor network has a label a=1,2,3,4. The label 1 corresponds to a stripe of \mathbb{Z}_2 topological order in the trivial sector. The label 2,3,4 correspond to a stripe in the non-trivial sectors. Applying an open e-string operator W_e connecting the two boundaries to the trivial sector produces the sector-2 (see Fig. 6). Similarly, applying the open m-string (f-string) operator W_m (W_f) connecting the two boundaries to the trivial sector produces the sector-3 (the sector-4).

A ground state of the cellular topological phase is given by the stripes of \mathbb{Z}_2 topological orders, all in the trivial sector (*i.e.* with label a = 1 on all links). Now we apply

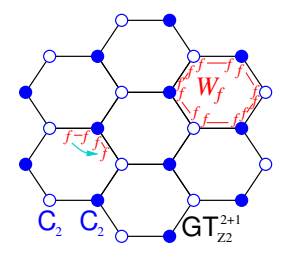


FIG. 10. In the cellular topological state $(\mathsf{GT}^{2+1}_{\mathbb{Z}_2},\mathsf{C}_2,\mathsf{C}_2)$, the f-particle can move freely in 3d space.

a loop e-string operators W_e^{loop} on some links to make them to be a small loop of sector-2 (see Fig. 8). The configuration corresponds to another degenerate ground state. Thus each hexagon contributes a factor 2 to the ground state degeneracy.

When the separation between vertices is small, the operators W_e^{loop} are local operators. We may include such operators in the Hamiltonian $\delta H = J \sum W_e^{\text{loop}}$. The new Hamiltonian no longer commute with m-string operators W_m . So δH splits the ground state degeneracy. The new ground states is believed to have a finite degeneracy independent of system size.

The condensation $m_1m_2m_3$ at the 1+1D topological order C_1 implies that we can create three m-particles on the neighboring three 2+1D \mathbb{Z}_2 topological orders, which form a small triangle in the dual honeycomb lattice. Putting many small triangles together gives us a loop in the dual honeycomb lattice formed by the m-particles (see Fig. 9). However, the z-coordinates of the m-particles can be arbitrary.

But if we add the $\delta H = J \sum W_e^{\text{loop}}$ term to the Hamiltonian, it will confine two m-particles in the same stripe of the \mathbb{Z}_2 topological order. In this case the above loop of the m-particles must have similar z-coordinates, in order to reduce the energy.

Those properties suggest that the cellular topological state $(\mathsf{GT}^{2+1}_{\mathbb{Z}_2},\mathsf{C}_1,\mathsf{C}_1)$ is a 3+1D \mathbb{Z}_2 topological order $\mathsf{GT}^{3+1}_{\mathbb{Z}_2}$. The free-moving e-particle is the point-like \mathbb{Z}_2 -charge in $\mathsf{GT}^{3+1}_{\mathbb{Z}_2}$. The loop of m-particles is the \mathbb{Z}_2 -flux loop in $\mathsf{GT}^{3+1}_{\mathbb{Z}_2}$.

C. Cellular topological state $(\mathsf{GT}^{2+1}_{\mathbb{Z}_2},\mathsf{C}_2,\mathsf{C}_2)$

The cellular topological state $(\mathsf{GT}^{2+1}_{\mathbb{Z}_2},\mathsf{C}_2,\mathsf{C}_2)$ is also a gapped liquid state – a 3+1D \mathbb{Z}_2^f topological ordered state $\mathsf{GT}^{3+1}_{\mathbb{Z}_2^f}$ described by twisted \mathbb{Z}_2 gauge theory where the point-like \mathbb{Z}_2 -charge is a fermion.⁸⁰

The 1+1D topological order C_2 has a condensation of $f_1f_2,\,f_2f_3,\,$ and $f_3f_1,\,$ for the excitations in the connected 2+1D topological orders. This means that the f-particles can freely move between the 2+1D topological orders $\mathsf{GT}^{2+1}_{\mathbb{Z}_2}$ connected by the 1+1D topological order C_2 (see

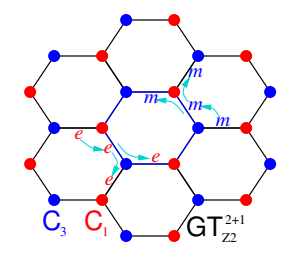


FIG. 11. In the cellular topological state $(\mathsf{GT}_{21}^{2+1}, \mathsf{C}_1, \mathsf{C}_3)$, the *e*-particle can move across the C_1 boundary, and the *m*-particle can move across the C_3 boundary. However, the long distant motion of *e*- and *m*-particles are blocked.

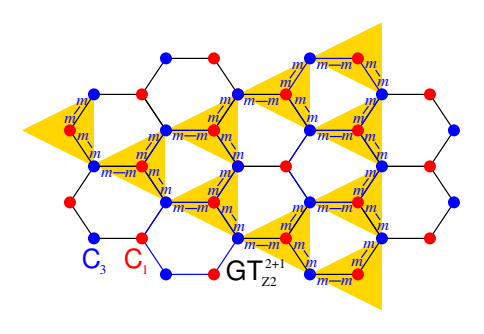


FIG. 12. A configuration in the ground state. The unmarked links are in sector-1. The links marked by m-m are in sector-3

Fig. 10). In other words, the f-particle can move freely in the whole 3d space, which corresponds to the point-like \mathbb{Z}_2 -charge in the 3+1D \mathbb{Z}_2^f topological order $\mathsf{GT}_{\mathbb{Z}_2^f}^{3+1}$. Similarly, the loop of m-particles is the \mathbb{Z}_2 -flux loop in $\mathsf{GT}_{\mathbb{Z}_2^f}^{3+1}$.

D. Cellular topological state $(GT_{\mathbb{Z}_2}^{2+1}, C_1, C_3)$

The cellular topological state $(\mathsf{GT}^{2+1}_{\mathbb{Z}_2},\mathsf{C}_1,\mathsf{C}_3)$ is a gapped non-liquid state, which is a fracton state with fractal excitations. In such a cellular topological state, e-particle (m-particle) can move across the C_1 (C_3) boundaries (see Fig. 11). But the motion of e-particle (m-particle) is blocked by the C_3 (C_1) boundaries. To move across the C_3 (C_1) boundaries, the e-particle (m-particle) must split into two (see Fig. 11). So the e- and m-particles cannot move freely in x-y direction, indicating that the cellular topological state maybe a non-liquid state. However, the e-particle and m-particle can move freely in z-direction within a stripe of \mathbb{Z}_2 topological order (see Fig. 9).

Remember that a ground state of the cellular topological phase is given by the stripes of \mathbb{Z}_2 topological orders, all in the trivial sector (i.e. with label a=1 on all links). Now we apply the m-string operators W_m on some links to make them to be the sector-3. The created m-particle

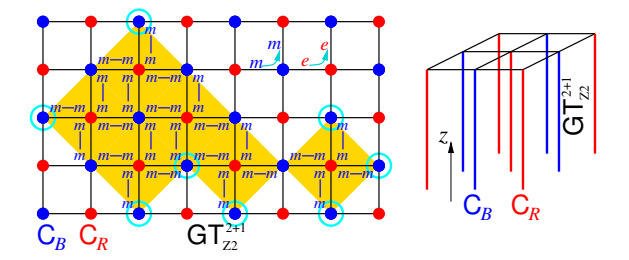


FIG. 13. A configuration of the cellular topological state. The unmarked links are in sector-1. The links marked by m-m are in sector-3. Only the vertices in the blue circle cost energy.

bound state on a vertex must be able to condense on the boundary. In this case, we create another degenerate ground state (see Fig. 12). We can also apply the e-string operators W_e on some links to make them to be the sector-2. The created e-particle bound state on the boundary must be able to condense on the boundary (the resulting configuration is similar to Fig. 12). This way, we obtain another degenerate ground state. We can also apply the e-string and m-string operators together to obtain new degenerate ground states. Counting all such configurations give us the ground state degeneracy. We note that different degenerate ground states have a large separation of code distance, which increases with system size.

From Fig. 12, we see that, in the ground state, the links in sector-3 form many small triangles. A corner of a triangle must connect to one and only one corner of another triangle. This way, the links in sector-3 form a fractal (see Fig. 12). This implies that the cellular topological state $(\mathsf{GT}^{2+1}_{\mathbb{Z}_2},\mathsf{C}_1,\mathsf{C}_3)$ is a fracton state with fractal excitations.

If a corner of a triangle is not connected to any corner triangle, such a corner will represent a point-like excitation. But the x-y motion for such a point-like excitation is highly restricted, like the point excitations in Haah's cubic code. Such kind of point excitations are called fractons. We see fractons are created at the corners of the fractal operator. However, fractons can move freely in the z-direction within a stripe of \mathbb{Z}_2 topological order.

We believe that the cellular topological states, $(\mathsf{GT}^{2+1}_{\mathbb{Z}_2},\mathsf{C}_1,\mathsf{C}_2), \quad (\mathsf{GT}^{2+1}_{\mathbb{Z}_2},\mathsf{C}_1,\mathsf{C}_4), \quad (\mathsf{GT}^{2+1}_{\mathbb{Z}_2},\mathsf{C}_2,\mathsf{C}_3), \\ (\mathsf{GT}^{2+1}_{\mathbb{Z}_2},\mathsf{C}_3,\mathsf{C}_4), \text{ are similar to the cellular topological states } (\mathsf{GT}^{2+1}_{\mathbb{Z}_2},\mathsf{C}_1,\mathsf{C}_3) \text{ discussed above. They should also be fracton states with fractal excitations.}$

E. A cellular topological state on square column lattice

In this section we consider a cellular topological state on a lattice formed by square columns (see Fig. 13). The stripes in the z-direction are occupied by $2+1D \mathbb{Z}_2$

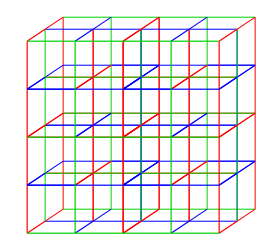


FIG. 14. A cellular topological state on cubic lattice. The square faces are occupied by 2+1D \mathbb{Z}_2 topological order, and the red, blue, green lines correspond to three kinds of 1+1D anomalous topological orders C_R , C_B , and C_G . For example, we assign the anomalous topological orders C_R and C_B to the links in the x-direction in an alternative way.

topological order. The red and blue vertical lines are two kinds of boundaries, C_R and C_B , of those \mathbb{Z}_2 topological orders:

$$\begin{aligned} &\mathsf{Bulk}(\mathsf{C}_R) = \mathsf{GT}_{\mathbb{Z}_2}^{2+1} \boxtimes \mathsf{GT}_{\mathbb{Z}_2}^{2+1} \boxtimes \mathsf{GT}_{\mathbb{Z}_2}^{2+1} \boxtimes \mathsf{GT}_{\mathbb{Z}_2}^{2+1}, \\ &\mathsf{Bulk}(\mathsf{C}_B) = \mathsf{GT}_{\mathbb{Z}_2}^{2+1} \boxtimes \mathsf{GT}_{\mathbb{Z}_2}^{2+1} \boxtimes \mathsf{GT}_{\mathbb{Z}_2}^{2+1} \boxtimes \mathsf{GT}_{\mathbb{Z}_2}^{2+1}. \end{aligned} \tag{21}$$

The two boundaries are characterized by the following condensing topological excitations (the generators):

$$C_R: e_1e_2, e_1e_3, e_1e_4, m_1m_2m_3m_4, f_1f_2f_3f_4,$$

 $C_B: m_1m_2, m_1m_3, m_1m_4, e_1e_2e_3e_4, f_1f_2f_3f_4.$ (22)

From the condensing particles on the boundaries, we see that the e-particle can move across the C_R boundaries, while the m-particle can move across the C_B boundaries. But, the arrangement of the C_R and C_B boundaries is such that the long distant motion of the e-and m-particles is blocked and they cannot move freely in the x-y direction. This suggests the cellular topological state to be a non-liquid state.

If all the links are in sector-1, then we have a minimal energy ground state. If we change some links to sector-3 (marked by m-m in Fig. 13), we will get an excited state. We may group the sector-3 links into small diamonds (see Fig. 13). Only the vertices that touch an odd number of the diamonds cost a finite energy (see Fig. 13), and correspond to a fracton. A fracton cannot move by itself in x-y directions. Only a pair of fractons can move in a certain way in x-y directions. But a fracton can move freely and independently in z-direction. The fractons are created at the corner of diamond-shaped membrane operators. Those properties suggests that the constructed cellular topological state is a type-I fracton state.

F. A cellular topological state on cubic lattice

Now, we consider a cellular topological state on a cubic lattice columns (see Fig. 14), which is a generalization of the square column model in the last section. The square

faces of the cubic lattice are occupied by 2+1D \mathbb{Z}_2 topological order. The red, blue, and green lines are three kinds of boundaries, C_R , C_B , and C_G of those \mathbb{Z}_2 topological orders:

$$\begin{split} & \mathsf{Bulk}(\mathsf{C}_R) = \mathsf{GT}_{\mathbb{Z}_2}^{2+1} \boxtimes \mathsf{GT}_{\mathbb{Z}_2}^{2+1} \boxtimes \mathsf{GT}_{\mathbb{Z}_2}^{2+1} \boxtimes \mathsf{GT}_{\mathbb{Z}_2}^{2+1}, \\ & \mathsf{Bulk}(\mathsf{C}_B) = \mathsf{GT}_{\mathbb{Z}_2}^{2+1} \boxtimes \mathsf{GT}_{\mathbb{Z}_2}^{2+1} \boxtimes \mathsf{GT}_{\mathbb{Z}_2}^{2+1} \boxtimes \mathsf{GT}_{\mathbb{Z}_2}^{2+1}, \\ & \mathsf{Bulk}(\mathsf{C}_G) = \mathsf{GT}_{\mathbb{Z}_2}^{2+1} \boxtimes \mathsf{GT}_{\mathbb{Z}_2}^{2+1} \boxtimes \mathsf{GT}_{\mathbb{Z}_2}^{2+1} \boxtimes \mathsf{GT}_{\mathbb{Z}_2}^{2+1}. \end{split} \tag{23}$$

The above three boundaries are characterized by the following condensing topological excitations (the generators):

$$C_R: e_1e_2, e_1e_3, e_1e_4, m_1m_2m_3m_4, f_1f_2f_3f_4,$$
 $C_B: m_1m_2, m_1m_3, m_1m_4, e_1e_2e_3e_4, f_1f_2f_3f_4,$
 $C_G: f_1f_2, f_1f_3, f_1f_4, e_1e_2e_3e_4, m_1m_2m_3m_4.$ (24)

From the condensing particles on the boundaries, we see that the e-particle can move across the C_R boundaries, the m-particle can move across the C_B boundaries, and the f-particle can move across the C_G boundaries. But, the arrangement of the C_R , C_B , and C_G boundaries is such that the long distant motion of the e-, m-, and f-particles is blocked and they cannot move freely in the any directions. In other words, they are localized in a finite region. To move further, those particles must split into more and more particles. This suggests the cellular topological state in Fig. 14 to be a non-liquid state. In particular, the structure described in Fig. 13 also appears in the cubic cellular model, and gives rise to point-like excitations with constrained motion.

IV. REVERSE RENORMALIZATION AND GENERIC CONSTRUCTION

To systematically understand and to classify a gapped liquid state (such as a topologically ordered state), we perform wavefunction renormalization by removing the unentangled degrees of freedom.^{78,81–83} We hope to obtain a fixed-point wave function which gives us a classifying understanding of the gapped liquid states. We also hope the fixed-point wave function is described by a topological quantum field theory which does not dependent on the lattice details.

However, for gapped non-liquid states, due to their intrinsic foliation or cellular structure, above general approach does not work. In particular, we should not expect to have a quantum field theory to describe a nonliquid state. (But a quantum field theories with explicit layer structure may work.⁵³) On the other hand, we still hope to obtain some kind of fixed-point wave functions for non-liquid states, so that we can have a systematic and classifying understanding of non-liquid states.

Here we like to propose a reverse renormalization approach to obtain the fixed-point wave functions for nonliquid states. In such an approach, we add unentangled degrees of freedom to our systems, to separation the layers in the foliation or cellular structure. After many steps of renormalization, we get 3+1D gapped liquid states between layers (i.e. within a cell), such as topologically ordered states or SET/SPT states if we have symmetry. (In our previous discussions, we have assumed the 3+1D gapped liquid states to be trivial product states.) On the layers, we have 2+1D anomalous topological orders, which are the domain walls separating the neighboring 3+1D topological orders. The layers join at edges, which correspond to 1+1D anomalous topological orders. The edges join at vertices, which correspond to 0+1D anomalous topological orders (see Fig. 1).

The above reverse renomalization understanding of non-liquid states suggests the following general construction. We first decompose the 3d space into cells (see Fig. 1). We assign (possibly different) 3+1D topological orders to the 3d cells, assign 2+1D anomalous topological orders to the 2d surfaces, assign 1+1D anomalous topological orders to the 1d edges, and assign 0+1D anomalous topological orders to the 0d vertices. (Without symmetry, the 0+1D anomalous topological orders are always trivial. 42) This is a quite general construction, which may cover all the non-liquid states. However, some constructions may give rise to ground state degeneracies that can be lifted by local operators. We need to include those local operators to lift the degeneracies and to stabilize the constructed states. Also, different constructions may lead to the same gapped non-liquid phase. Finding the equivalence relations between different constructions is an every important issue.

Our construction also works if there are on-site symmetry, by requiring the (anomalous) topological orders in various dimensions to have the same symmetry. In the presence of space group symmetry, we need to choose the cellular structure to have the space group symmetry. We also need to choose (anomalous) topological orders in various dimensions to have the proper symmetries, as discussed in Ref. 45–48.

After posting this paper, the author became aware of a prior unpublished work (now posted as Ref. 84) where a very similar construction, based on defect network in a 3+1D topological quantum field theory, was proposed. The defect planes and defect lines correspond to the (anomalous) 2+1D and 1+1D topological orders in this paper. Later, another similar construction was proposed in Ref. 85.

I would like to thank Xie Chen and Kevin Slagle to bring the above work to my attention. This work is motivated by the presentations in the Annual Meeting of Simons Collaboration on Ultra-Quantum Matter, where the issue of the fixed point field theory for fracton phases were discussed. This research was partially supported by NSF DMS-1664412. This work was also partially supported by the Simons Collaboration on Ultra-Quantum Matter, which is a grant from the Simons Foundation (651440).

- ¹ L. D. Landau, Phys. Z. Sowjetunion **11**, 26 (1937).
- ² L. D. Landau, Phys. Z. Sowjetunion **11**, 545 (1937).
- ³ X. Chen, Z.-C. Gu, and X.-G. Wen, Phys. Rev. B 82, 155138 (2010), arXiv:1004.3835.
- ⁴ B. Zeng and X.-G. Wen, Phys. Rev. B **91**, 125121 (2015), arXiv:1406.5090.
- ⁵ B. Swingle and J. McGreevy, Phys. Rev. B **93**, 045127 (2016), arXiv:1407.8203.
- ⁶ X.-G. Wen, Phys. Rev. B **40**, 7387 (1989).
- ⁷ X.-G. Wen, Int. J. Mod. Phys. B **04**, 239 (1990).
- ⁸ E. Keski-Vakkuri and X.-G. Wen, Int. J. Mod. Phys. B 07, 4227 (1993).
- ⁹ X.-G. Wen, Phys. Rev. B **65**, 165113 (2002), cond-mat/0107071.
- ¹⁰ A. M. Essin and M. Hermele, Phys. Rev. B **87**, 104406 (2013), arXiv:1212.0593.
- ¹¹ L.-Y. Hung and Y. Wan, Phys. Rev. B 87, 195103 (2013), arXiv:1302.2951.
- 12 C. Xu, Phys. Rev. B $\pmb{88},\,205137$ (2013), arXiv:1307.8131.
- ¹³ A. Mesaros and Y. Ran, Phys. Rev. B 87, 155115 (2013), arXiv:1212.0835.
- ¹⁴ X. Chen, F. J. Burnell, A. Vishwanath, and L. Fidkowski, Phys. Rev. X 5, 041013 (2015), arXiv:1403.6491.
- ¹⁵ L. Chang, M. Cheng, S. X. Cui, Y. Hu, W. Jin, R. Movas-sagh, P. Naaijkens, Z. Wang, and A. Young, J. Phys. A: Math. Theor. 48, 12FT01 (2015), arXiv:1412.6589.
- ¹⁶ M. Cheng, Z.-C. Gu, S. Jiang, and Y. Qi, Phys. Rev. B 96, 115107 (2017), arXiv:1606.08482.
- ¹⁷ C. Heinrich, F. Burnell, L. Fidkowski, and M. Levin, Phys. Rev. B **94**, 235136 (2016), arXiv:1606.07816.
- ¹⁸ Z.-C. Gu and X.-G. Wen, Phys. Rev. B **80**, 155131 (2009), arXiv:0903.1069.
- ¹⁹ X. Chen, Z.-X. Liu, and X.-G. Wen, Phys. Rev. B 84, 235141 (2011), arXiv:1106.4752.
- ²⁰ X. Chen, Z.-C. Gu, Z.-X. Liu, and X.-G. Wen, Phys. Rev. B 87, 155114 (2013), arXiv:1106.4772.
- ²¹ C. Chamon, Phys. Rev. Lett. **94**, 040402 (2005).
- ²² J. Haah, Phys. Rev. A **83**, 042330 (2011), arXiv:1101.1962.
- ²³ W. Shirley, K. Slagle, Z. Wang, and X. Chen, Phys. Rev. X 8, 031051 (2018), arXiv:1712.05892.
- ²⁴ W. Shirley, K. Slagle, and X. Chen, SciPost Phys. 6, 015 (2019), arXiv:1803.10426.
- ²⁵ S. Vijay, J. Haah, and L. Fu, Phys. Rev. B **94**, 235157 (2016), arXiv:1603.04442.
- ²⁶ X. Chen, Z.-C. Gu, and X.-G. Wen, Phys. Rev. B 83, 035107 (2011), arXiv:1008.3745.
- ²⁷ N. Schuch, D. Pérez-García, and I. Cirac, Phys. Rev. B 84, 165139 (2011), arXiv:1010.3732.
- ²⁸ M. Barkeshli, P. Bonderson, M. Cheng, and Z. Wang, (2014), arXiv:1410.4540.
- ²⁹ T. Lan, L. Kong, and X.-G. Wen, Phys. Rev. B **95**, 235140 (2017), arXiv:1602.05946.
- ³⁰ T. Lan, L. Kong, and X.-G. Wen, Commun. Math. Phys. 351, 709 (2016), arXiv:1602.05936.
- ³¹ T. Lan, L. Kong, and X.-G. Wen, Phys. Rev. X 8, 021074 (2018), arXiv:1704.04221.
- ³² T. Lan and X.-G. Wen, Phys. Rev. X 9, 021005 (2019), arXiv:1801.08530.
- ³³ C. Zhu, T. Lan, and X.-G. Wen, Phys. Rev. B **100**, 045105 (2019), arXiv:1808.09394.
- ³⁴ A. Kapustin, (2014), arXiv:1404.6659.

- ³⁵ Z.-C. Gu and X.-G. Wen, Phys. Rev. B **90**, 115141 (2014), arXiv:1201.2648.
- ³⁶ A. Kapustin, R. Thorngren, A. Turzillo, and Z. Wang, J. High Energ. Phys. **2015**, 1 (2015), arXiv:1406.7329.
- ³⁷ D. Gaiotto and A. Kapustin, Int. J. Mod. Phys. A **31**, 1645044 (2016), arXiv:1505.05856.
- ³⁸ D. S. Freed and M. J. Hopkins, (2016), arXiv:1604.06527.
- ³⁹ A. Kapustin and R. Thorngren, J. High Energ. Phys. **2017**, 80 (2017), arXiv:1701.08264.
- ⁴⁰ Q.-R. Wang and Z.-C. Gu, Phys. Rev. X 8, 011055 (2018), arXiv:1703.10937.
- ⁴¹ M. Pretko, X. Chen, and Y. You, International Journal of Modern Physics A 35, 2030003 (2020), arXiv:2001.01722.
- ⁴² L. Kong and X.-G. Wen, (2014), arXiv:1405.5858.
- ⁴³ X.-G. Wen, Phys. Rev. D 88, 045013 (2013), arXiv:1303.1803.
- ⁴⁴ A. Kapustin, (2014), arXiv:1403.1467.
- ⁴⁵ X. Chen, Y.-M. Lu, and A. Vishwanath, Nat Commun 5, 4507 (2014), arXiv:1303.4301.
- ⁴⁶ H. Song, S.-J. Huang, L. Fu, and M. Hermele, Phys. Rev. X 7, 011020 (2017), arXiv:1604.08151.
- ⁴⁷ S.-J. Huang, H. Song, Y.-P. Huang, and M. Hermele, Phys. Rev. B **96**, 205106 (2017), arXiv:1705.09243.
- ⁴⁸ Z. Song, C. Fang, and Y. Qi, (2018), arXiv:1810.11013.
- ⁴⁹ H. Ma, E. Lake, X. Chen, and M. Hermele, Phys. Rev. B 95, 245126 (2017), arXiv:1701.00747.
- ⁵⁰ K. Slagle and Y. B. Kim, Phys. Rev. B **96**, 165106 (2017), arXiv:1704.03870.
- ⁵¹ S. Vijay, (2017), arXiv:1701.00762.
- ⁵² A. Prem, S.-J. Huang, H. Song, and M. Hermele, Physical Review X 9, 021010 (2019), arXiv:1806.04687.
- ⁵³ K. Slagle, D. Aasen, and D. Williamson, SciPost Physics 6, 043 (2019), arXiv:1812.01613.
- ⁵⁴ Y. Fuji, Phys. Rev. B **100**, 235115 (2019) arXiv:1908.02257.
- ⁵⁵ C. Xu, (2006), cond-mat/0602443.
- ⁵⁶ Z.-C. Gu and X.-G. Wen, (2006), gr-qc/0606100.
- ⁵⁷ Z.-C. Gu and X.-G. Wen, Nucl. Phys. B **863**, 90 (2012), arXiv:0907.1203.
- ⁵⁸ T. Lan and X.-G. Wen, Phys. Rev. B **90**, 115119 (2014), arXiv:1311.1784.
- ⁵⁹ T. Lan, J. C. Wang, and X.-G. Wen, Phys. Rev. Lett. 114, 076402 (2015), arXiv:1408.6514.
- ⁶⁰ Y. Hu, Y. Wan, and Y.-S. Wu, Chinese Physics Letters 34, 077103 (2017), arXiv:1706.00650.
- ⁶¹ T. Lan, X. Wen, L. Kong, and X.-G. Wen, (2019), arXiv:1911.08470.
- ⁶² L. Kong, X.-G. Wen, and H. Zheng, (2015), arXiv:1502.01690.
- ⁶³ L. Kong, X.-G. Wen, and H. Zheng, Nucl. Phys. B **922**, 62 (2017), arXiv:1702.00673.
- ⁶⁴ L. Kong, T. Lan, X.-G. Wen, Z.-H. Zhang, and H. Zheng, (2020), arXiv:2005.14178.
- ⁶⁵ A. Kapustin and N. Saulina, Nucl. Phys. B **845**, 393 (2011), arXiv:1008.0654.
- ⁶⁶ A. Kitaev and L. Kong, Commun. Math. Phys. **313**, 351 (2012), arXiv:1104.5047.
- ⁶⁷ J. C. Wang and X.-G. Wen, Phys. Rev. B **91**, 125124 (2015), arXiv:1212.4863.
- ⁶⁸ L. Kong, Nucl. Phys. B **886**, 436 (2014), arXiv:1307.8244.
- ⁶⁹ L.-Y. Hung and Y. Wan, Int. J. Mod. Phys. B **28**, 1450172

- (2014), arXiv:1308.4673.
- ⁷⁰ L.-Y. Hung and Y. Wan, Phys. Rev. Lett. **114**, 076401 (2015), arXiv:1408.0014.
- ⁷¹ M. Mignard and P. Schauenburg, (2017),arXiv:1708.02796.
- 72 P. Bonderson, C. Delaney, C. Galindo, E. C. Rowell, A. Tran, and Z. Wang, (2018), arXiv:1805.05736.
- 73 X. Wen and X.-G. Wen, (2019), arXiv:1908.10381.
 74 E. Rowell, R. Stong, and Z. Wang, Commun. Math. Phys. 292, 343 (2009), arXiv:0712.1377.
- ⁷⁵ X.-G. Wen, Nat. Sci. Rev. **3**, 68 (2015), arXiv:1506.05768.
- ⁷⁶ N. Read and S. Sachdev, Phys. Rev. Lett. **66**, 1773 (1991).
- ⁷⁷ X.-G. Wen, Phys. Rev. B **44**, 2664 (1991).

- ⁷⁸ F. Verstraete and J. I. Cirac, (2004), cond-mat/0407066.
- ⁷⁹ M. Levin and C. P. Nave, Phys. Rev. Lett. **99**, 120601
- ⁸⁰ M. Levin and X.-G. Wen, Phys. Rev. B **67**, 245316 (2003), cond-mat/0302460.
- ⁸¹ G. Vidal, Phys. Rev. Lett. **99**, 220405 (2007).
 ⁸² M. Aguado and G. Vidal, Phys. Rev. Lett. **100**, 070404 (2008).
- 83 Z.-C. Gu, M. Levin, and X.-G. Wen, Phys. Rev. B 78, 205116 (2008), arXiv:0806.3509.
- ⁸⁴ D. Aasen, B. Bulmash, A. Prem, K. Slagle, and D. J. Williamson, (2020), arXiv:2002.05166.
- 85 J. Wang, (2020), arXiv:2002.12932.